Eur. Phys. J. C (2024) 84:1295
https://doi.org/10.1140/epjc/s10052-024-13661-1

THE EUROPEAN PHYSICAL JOURNAL C

Regular Article - Theoretical Physics

Stability of compact stars in a uniform density background cloud

Ksh. Newton Singh[1,a], **S. K. Maurya**[2,3,b], **A. Errehymy**[4,c], **O. Donmez**[5,d], **K. Myrzakulov**[6,e], **T. T. Smitha**[2,f]

[1] Department of Physics, National Defence Academy, Khadakwasla, Pune 411023, India
[2] Department of Mathematical and Physical Sciences, College of Arts and Sciences, University of Nizwa, 616 Nizwa, Sultanate of Oman
[3] Research Center of Astrophysics and Cosmology, Khazar University, 41 Mehseti Street, AZ1096 Baku, Azerbaijan
[4] Astrophysics Research Centre, School of Mathematics, Statistics and Computer Science, University of KwaZulu-Natal, Private Bag X54001, Durban 4000, South Africa
[5] College of Engineering and Technology, American University of the Middle East, 54200 Egaila, Kuwait
[6] Department of General and Theoretical Physics, L.N. Gumilyov Eurasian National University, 010008 Astana, Kazakhstan

Received: 8 September 2024 / Accepted: 28 November 2024 / Published online: 20 December 2024

Abstract We are discussing a scenario where a compact star (neutron star, NS) is embedded in a thin, uniform density background cloud (a remnant cloud after a supernova or a cloud generated from the late stages of a star e.g., a planetary nebula or asymptotic red giant phases) and its effect on the stability of the compact star. Due to the thin background cloud, the spacetime geometry is minimally deformed allowing us to employ the technique of minimal geometric decoupling (MGD). Assuming a uniform background cloud density simplifies the problem, and through the MGD method, one can take $\Theta_t^t = \Theta > 0$, where Θ is the density of the cloud. The background cloud interacts with the compact star through a coupling strength α. By varying α, one can tune the cloud density to analyze the stability of the embedded compact star. We found that for $\alpha < 3 \times 10^{-5}$, all the thermodynamic quantities are well-behaved, indicating a stable configuration. Once the coupling parameter exceeds 3×10^{-5}, the adiabatic index drops below $\Gamma'_{\rm max}$, triggering a gravitational collapse. Beyond this limit of α, the pressure and speed of sound also become non-physical. At the end, we have used the $M-R$ curve generated from the solution to determine the radii of a few compact stars, namely PSR J1614-2230, PSR J0952-0607, GW190814, and GW200210. Furthermore, we have discussed the possibility of the secondary component of GW200210 i.e. the less massive compact object with an upper mass of $3.3M_\odot$, which may be a stellar black hole with a Schwarzschild radius $R_{\rm BH} = 9.746$ km. However, if the mass is $2.83M_\odot$ as observed, then its predicted minimum radius is 10.74 km, corresponding to $\alpha = 0$. This radius is far beyond $R_{\rm BH} = 8.357$ km and therefore is most probably a massive NS in the mass gap.

1 Introduction

A NS is one of the most compact and dense forms of matter in the observable cosmos. It is formed by the gravitational collapse of the central core of a massive star (typically with a mass greater than eight times the mass of our Sun) at the end of its lifetime. This collapse is followed by a stellar phenomenon known as a supernova explosion [1]. The internal structure of NSs is determined by the nuclear equation of state (EOS) governing the behavior of matter at these extreme densities. These incredibly compact stellar remnants can be detected through various observational techniques, typically involving optical and X-ray astronomy [2]. However, our theoretical understanding of cold, ultradense matter remains imperfect, as the conditions found within NSs currently exceed the capabilities of existing laboratory experiments to replicate [3].

The community often employs meta-models that encompass the whole permissible pressure-energy density or mass-radius parameter space, owing to our ignorance of the EOS for extreme densities and highly asymmetric matter, or the emergence of unusual degrees of freedom. Several approaches have been employed to put this concept into practice [4–6]. These include parameterizing the EOS using poly-

[a] e-mail: ntnphy@gmail.com
[b] e-mail: sunil@unizwa.edu.om
[c] e-mail: abdelghani.errehymy@gmail.com (corresponding author)
[d] e-mail: orhan.donmez@aum.edu.kw
[e] e-mail: krmyrzakulov@gmail.com (corresponding author)
[f] e-mail: smitha@unizwa.edu.om

tropes [7–10], the speed of sound [11–15], or spectral representations [16–18] – techniques that can impose causality constraints when necessary. More recently, Gaussian processes were introduced [19,20] as a non-parametric modeling method.

The existing methods allow us to constrain the EOS domain that matches observational data, but they do not provide any insights into the composition of the matter, including the proton fraction or the presence of non-nucleonic degrees of freedom like hyperons, delta baryons, or deconfined quark matter. These compositional details remain unknown and require further investigation to fully characterize the properties of the dense matter under study. In the current study, we shall imagine a scenario where a NS is surrounded by a thin, uniform cloud (remnant of a supernova or cloud generated from the late stages of a star, e.g., planetary nebula or asymptotic red giant phases), and investigate how the stability of the NS can be altered due to the addition of small mass from the thin cloud through the accretion process. Therefore, we will employ the technique of gravitational decoupling minimal via geometric deformation (MGD) to handle the minimally deformed spacetime geometry caused by the thin background cloud. The GD technique through the MGD was introduced by Ovalle [21], which is an innovative method that enables the anisotropization of well-established isotropic solutions or generalization of any known anisotropic solution of the Einstein field equations (EFEs). The MGD allows us to split the original system into two subsystems, namely the seed system, which is the same as the Einstein general relativity (GR) system for source $\hat{T}_{\mu\nu}$, while the other system corresponds to source $\Theta_{\mu\nu}$, which is known as the quasi-Einstein system. This means that this methodology includes a new source $\Theta_{\mu\nu}$ into the seed energy–momentum tensor $\tilde{T}_{\mu\nu}$ of the conventional EFEs. Including $\Theta_{\mu\nu}$ can serve as a source of anisotropy, dark matter, or density cloud. The MGD has enabled researchers to investigate new solutions or extensions of known solutions of EFEs from the isotropic to the anisotropic domain or new solutions in dark matter halos. The GD approach is not limited to GR, as it is also applicable for modified gravity theory [22–32].

Notably, the isotropic seed solution may lack physical viability, yet its anisotropic counterpart via GD processes may represent physically realizable structures. The foundation of GD in this approach is based on assuming a straightforward matter distribution ($\tilde{T}_{\mu\nu}$) and then extrapolating to a more intricate source while maintaining spherical symmetry. We can write

$$T_{\mu\nu} = \tilde{T}_{\mu\nu} + \alpha\,\Theta_{\mu\nu}.$$

The decoupling constant, α, connects conventional matter, $\tilde{T}_{\mu\nu}$, to the supplementary source $\Theta_{\mu\nu}$. We may proceed with this approach via a sequence of iterations as

$$\tilde{T}_{\mu\nu} = \tilde{T}^1_{\mu\nu} + \sigma\,\Theta^1_{\mu\nu},$$

that can generate more generalized gravitational fields. This is an innovative method to induce anisotropy in seed solutions obtained from ideal matter distributions.

Similarly, we may first consider the metric $g_{\mu\nu}$ corresponding to

$$\widetilde{G}_{\mu\nu} = \kappa^2\,\tilde{T}_{\mu\nu}, \tag{1}$$

to find the seed metric potential $\bar{g}_{\mu\nu}$ and then solve

$$G^{\Theta}_{\mu\nu} = \kappa^2\,\Theta_{\mu\nu}, \tag{2}$$

to generate the anisotropic source of metric $g^{\Theta}_{\mu\nu}$ where $\kappa^2 = 8\pi$ (in geometrical units $c = 1 = G$). The total EMT $T_{\mu\nu}$ can be decomposed as

$$T_{\mu\nu} = \tilde{T}_{\mu\nu} + \alpha\,\Theta_{\mu\nu}, \quad G_{\mu\nu} = \kappa^2\,T_{\mu\nu}, \tag{3}$$

where $\tilde{T}_{\mu\nu}$ represents the source energy–momentum tensor, and $\Theta_{\mu\nu}$ denotes an extra gravitational anisotropic source of energy–momentum tensor. Upon solving both sources individually, we may derive the metric $g_{\mu\nu}$ by combining $\tilde{g}_{\mu\nu}$ and $g^{\Theta}_{\mu\nu}$. This operation may be performed multiple times as the stated number of gravitational sources permits. In every cycle, we must infer the energy–momentum tensor (EMT) and include the corresponding gravitational potentials of the whole EMT. This technique demonstrates the rigorous work on the MGD and its extension, as demonstrated in the following references [33–37]. The MGD also works for the non-uniform cloud density but we have to choose the form of cloud density such that the overall magnitude of the deformation function should be increased with r to have a decreasing effective density of the system.

Assuming a uniform background cloud density, we can take $\Theta^t_t = \Theta > 0$, where Θ is the density of the cloud. The background cloud interacts with the compact star through a coupling strength α, and by varying α, we can tune the cloud density to analyze the stability of the embedded compact star. We will explore the range of α where all the thermodynamic quantities are well-behaved and represent a stable configuration. However, we will also look at whether the surrounding cloud density is at least 5% of the surface density of the NS or not, as this would indicate that the additional mass from the cloud has become significant in altering the stability of the NS. Furthermore, we will observe that the denser the cloud, the more mass can be added, and hence, the greater the pressure at the interior. Finally, we will explore whether the compact object in GW200210 with an upper mass of $3.3M_{\odot}$ could be confused with a stellar black hole having a Schwarzschild radius of $R_{BH} = 9.746$ km, or if it is more likely a massive NS, given that a mass of $2.83M_{\odot}$ would

correspond to a predicted radius of 10.74 km, which is far beyond the Schwarzschild radius of $R_{BH} = 8.357$ km, suggesting that it is indeed a massive NS in the mass-gap region.

The investigations are organized across seven main sections. Section 2 briefly outlines the standard field equations in geometric decoupling. In Sect. 3, a generalized compact star solution in a uniform density cloud is presented. Section 4 discusses the process of fixing multiple parameters via Schwarzschild vacuum, taking into account the extremely thin cloud density. The rigorous analysis and multiple tests are logically structured in various sub-sections of Sect. 5. Section 6 checks whether the solution is adapted to the observed astrophysical scenario via the $M-R$ curve. Finally, the final remarks are reported in Sect. 7.

2 Field equations in geometric decoupling

The Einstein–Hilbert action in pure general relativity is modified by adding a geometric decoupling term as follows [38]

$$S = \int \left[\frac{\mathcal{R}}{16\pi} + \mathcal{L}_M + \alpha\,\mathcal{L}_\Theta\right]\sqrt{-g}\,d^4x. \tag{4}$$

Here, $\mathcal{L}_M$ represents the matter field Lagrangian density, and $\mathcal{L}_\Theta$ denotes the Lagrangian density induced by the extra source that produces the GD. The Ricci invariant is denoted by $\mathcal{R}$, and α is the coupling strength. The energy–momentum tensors for $\mathcal{L}_M$ and $\mathcal{L}_\Theta$ are given by

$$\tilde{T}_{\mu\nu} = -\frac{2}{\sqrt{-g}}\frac{\delta(\sqrt{-g}\,\mathcal{L}_M)}{\delta g^{\mu\nu}} = g_{\mu\nu}\mathcal{L}_M - \frac{2\,\partial\mathcal{L}_M}{\partial g^{\mu\nu}}, \tag{5}$$

$$\Theta_{\mu\nu} = -\frac{2}{\sqrt{-g}}\frac{\delta(\sqrt{-g}\,\mathcal{L}_\Theta)}{\delta g^{\mu\nu}} = g_{\mu\nu}\mathcal{L}_\Theta - 2\frac{\delta\mathcal{L}_\Theta}{\delta g^{\mu\nu}}. \tag{6}$$

Here $\Theta^{\nu}_{\mu} = \text{diag}(\Theta^t_t, \Theta^r_r, \Theta^\theta_\theta, \Theta^\phi_\phi)$ is the stress-tensor corresponding to the extra source term that generates the geometric deformation. Varying (4) with respect to $g^{\mu\nu}$, we obtain the general equations of motion

$$\mathcal{R}_{\mu\nu} - \frac{1}{2}g_{\mu\nu}\mathcal{R} = -8\pi\,T_{\mu\nu} = -8\pi(\tilde{T}_{\mu\nu} + \alpha\,\Theta_{\mu\nu}). \tag{7}$$

Considering an anisotropic fluid matter $\tilde{T}_{\mu\nu}$ that is unperturbed by the GD, we have

$$\tilde{T}_{\mu\nu} = (\tilde{\rho} + \tilde{p}_t)u_\mu u_\nu - \tilde{p}_t g_{\mu\nu} + \left(\tilde{p}_r - \tilde{p}_t\right)v_\mu v_\nu. \tag{8}$$

All symbols have their usual meanings. The $\Theta_{\mu\nu}$ source term in Eq. (7) can introduce anisotropy in a self-gravitating system, which may be represented by a scalar, vector, or tensor field. Since the Einstein tensor is always divergence-free, the stress tensor $T_{\mu\nu}$ must also be divergence-free, i.e.

$$\nabla^\mu T_{\mu\nu} = 0. \tag{9}$$

For a spherically symmetric stellar system, the spacetime inside takes the form

$$ds^2 = e^{\nu(r)}dt^2 - e^{\lambda(r)}dr^2 - r^2\left(d\theta^2 + \sin^2\theta\,d\phi^2\right), \tag{10}$$

where ν and λ are functions of the radial coordinate 'r' only. The field equations (7) now reduce to

$$8\pi(\tilde{\rho} + \alpha\,\Theta^t_t) = \mathrm{e}^{-\lambda}\left(\frac{\lambda'}{r} - \frac{1}{r^2}\right) + \frac{1}{r^2}, \tag{11}$$

$$8\pi(\tilde{p}_r - \alpha\,\Theta^r_r) = \mathrm{e}^{-\lambda}\left(\frac{\nu'}{r} + \frac{1}{r^2}\right) - \frac{1}{r^2}, \tag{12}$$

$$8\pi(\tilde{p}_t - \alpha\,\Theta^\varphi_\varphi) = \frac{\mathrm{e}^{-\lambda}}{4}\left(2\nu'' + \nu'^2 + \frac{2(\nu' - \lambda')}{r} - \nu'\lambda'\right), \tag{13}$$

where the effective density (ρ), radial (p_r) & tangential pressure (p_t) and anisotropy are

$$\rho = \tilde{\rho} + \alpha\,\Theta^t_t \equiv \tilde{\rho} + \rho_\Theta, \tag{14}$$

$$p_r = \tilde{p}_r - \alpha\,\Theta^r_r, \tag{15}$$

$$p_t = \tilde{p}_t - \alpha\,\Theta^\varphi_\varphi, \tag{16}$$

$$\Delta = \tilde{p}_t - \tilde{p}_r + \alpha\,(\Theta^r_r - \Theta^\varphi_\varphi). \tag{17}$$

Further, the conservation equation $\nabla^\nu T^\mu_\nu = 0$ implies

$$-\frac{d\tilde{p}_r}{dr} - \frac{\nu'}{2}(\tilde{\rho} + \tilde{p}_r) + \frac{2(\tilde{p}_t - \tilde{p}_r)}{r} - \alpha\left[\frac{\nu'}{2}(\Theta^t_t - \Theta^r_r) - \frac{d\Theta^r_r}{dr} + \frac{2}{r}(\Theta^\varphi_\varphi - \Theta^r_r)\right] = 0, \tag{18}$$

which is the modified TOV equation.

2.1 Gravitational decoupling approach

Since the effective stress-energy tensor includes the source terms $\tilde{T}_{\mu\nu} + \alpha\,\Theta_{\mu\nu}$, the interior spacetime (10)

$$d\tilde{s}^2 = e^{\tilde{\nu}(r)}dt^2 - e^{\tilde{\lambda}(r)}dr^2 - r^2(d\theta^2 + \sin^2\theta\,d\phi^2), \tag{19}$$

where the gravitational potential $e^{\tilde{\lambda}(r)}$ can be defined as,

$$e^{-\tilde{\lambda}(r)} = 1 - \frac{8\pi}{r}\int_0^r r^2\,\rho(r)dr = 1 - \frac{2m(r)}{r}, \tag{20}$$

here the $m(r)$ represents the Misner–Sharp mass function for the standard GR. The influence of the extra source $\Theta_{\mu\nu}$ on the energy–momentum tensor $\tilde{T}_{\mu\nu}$ can be determined by the geometric deformation via perfect fluid geometry $\{\tilde{\nu}(r), \tilde{\lambda}(r)\}$ in Eq. (19) as

$$e^{\tilde{\nu}} \to e^{\nu} = e^{\tilde{\nu}} + \alpha\,f(r), \tag{21}$$

$$e^{-\tilde{\lambda}} \to e^{-\lambda} = e^{-\tilde{\lambda}} + \alpha\,g(r), \tag{22}$$

where $f(r)$ and $g(r)$ are the deformation functions associated with the temporal and radial components of line elements, respectively. It is noted that these deformation functions depend only on the radial coordinate, while the constant α is a free parameter. The considered MGD method allows us to set $g = 0$ or $f = 0$; in this situation, the deformation will be performed only on the radial component, while the temporal one remains unaltered (which corresponds to $f = 0$). By setting $f = 0$, we get

$$e^{-\tilde{\lambda}} \to e^{-\lambda} = e^{-\tilde{\lambda}} + \alpha\, g(r). \tag{23}$$

This is called the MGD along the radial component of the line element. After plugging the Eqs. (21) and (22) into the field equations (11)–(13), we get two sets of equations: (i) the standard Einstein field equations for an energy–momentum tensor $\tilde{T}_{\mu\nu}$, which are given as

$$\frac{1-e^{-\tilde{\lambda}}}{r^2} + \frac{e^{-\tilde{\lambda}}\tilde{\lambda}'}{r} = 8\pi\tilde{\rho}, \tag{24}$$

$$\frac{e^{-\tilde{\lambda}}-1}{r^2} + \frac{e^{-\tilde{\lambda}}\tilde{\nu}'}{r} = 8\pi\tilde{p}_r, \tag{25}$$

$$e^{-\tilde{\lambda}}\left(\frac{\tilde{\nu}''}{2} + \frac{\tilde{\nu}'^2}{4} - \frac{\tilde{\nu}'\tilde{\lambda}'}{4} + \frac{\tilde{\nu}'-\tilde{\lambda}'}{2r}\right) = 8\pi\tilde{p}_t. \tag{26}$$

along with the conservation equation,

$$-\frac{d\tilde{p}_r}{dr} - \frac{\nu'}{2}(\tilde{\rho}+\tilde{p}_r) + \frac{2(\tilde{p}_t-\tilde{p}_r)}{r} = 0, \tag{27}$$

while (ii) the set of equations for the source $\Theta_{\mu\nu}$, called the quasi-field equations, are given as

$$-\frac{g'}{r} - \frac{g}{r^2} = 8\pi\Theta_t^t, \tag{28}$$

$$-g\left(\frac{\tilde{\nu}'}{r} + \frac{1}{r^2}\right) = 8\pi\Theta_r^r, \tag{29}$$

$$-\frac{g}{2}\left(\tilde{\nu}'' + \frac{\tilde{\nu}'^2}{2} + \frac{\tilde{\nu}'}{r}\right) - \frac{g'}{2}\left(\frac{\tilde{\nu}'}{2} + \frac{1}{r}\right) = 8\pi\Theta_\varphi^\varphi. \tag{30}$$

The corresponding conservation equation $\nabla^\nu\Theta_{\mu\nu} = 0$ gives,

$$\frac{d\Theta_r^r}{dr} - \frac{\nu'}{2}(\Theta_t^t - \Theta_r^r) - \frac{2}{r}(\Theta_\varphi^\varphi - \Theta_r^r) = 0. \tag{31}$$

At this stage, it is noted that both sources $\tilde{T}\mu\nu$ and $\Theta\mu\nu$ are individually conserved, which implies that both systems interact only gravitationally.

3 Compact star solution in uniform density cloud

To begin, we need to turn off α and figure out how to solve Einstein's field equations (11)–(13) for an anisotropic fluid matter distribution, which is a seed system. To find the solution, we choose a well-known physically viable solution corresponding to the Krori–Barua (KB) metric ansatz [39]. There has been a lot of work done on the Krori–Barua spacetime to investigate static spherically compact objects in general relativity (GR) as well as in modified theories of gravity [40–43]. Here are the metric functions that describe the KB spacetime:

$$\tilde{\lambda} = c\,r^2 \quad \text{and} \quad \tilde{\nu} = a\,r^2 + b. \tag{32}$$

Next, we imagine a scenario where a compact star is surrounded by a thin uniform cloud, similar to a remnant cloud after a supernova or from a nearby late stage of a normal star. This scenario is quite possible in reality, as the last stage of a star is associated with the ejection of outer shells during evolution. This uniform-density cloud can minimally deform the spacetime, which can alter the properties of the compact star. The minimally deformed spacetime due to the background cloud will affect the field equations through Θ_ν^μ, and for uniform density, the $t-t$ component of the quasi-field equation (28) with $\Theta_t^t = \Theta > 0$ becomes

$$g'(r) + \frac{g(r)}{r} = -8\pi\, r\,\Theta \quad \text{or} \quad g(r) = \frac{C_1}{r} - \frac{8}{3}\pi\,\Theta\, r^2. \tag{33}$$

Here Θ is the background cloud density which is constant. To ensure the finiteness of the metric potential at $r = 0$, we have to take $C_1 = 0$; therefore, the deformation function becomes

$$g(r) = -\frac{8}{3}\pi\,\Theta\, r^2. \tag{34}$$

Now, the uniform-density cloud background deforms the unperturbed spacetime as follows

$$e^{\nu} = e^{\tilde{\nu}} = e^{ar^2+b} \quad \text{and} \quad e^{-\lambda} = e^{-cr^2} - \frac{8\pi\,\Theta\,\alpha}{3}\,r^2. \tag{35}$$

The modified thermodynamic variables take the form

$$\rho = \frac{e^{-c\,r^2}}{8\pi r^2}\left(2c\,r^2 + e^{c\,r^2} - 1\right) + \alpha\,\Theta, \tag{36}$$

$$p_r = \frac{1}{8\pi}\left\{\left(2a + \frac{1}{r^2}\right)e^{-c\,r^2} - \frac{1}{r^2}\right\} - \frac{\alpha\,\Theta}{3}\left(2ar^2 + 1\right), \tag{37}$$

$$p_t = \frac{e^{-c\,r^2}\left\{ar^2(a-c) + 2a - c\right\}}{8\pi} - \frac{\alpha\,\Theta}{3}\left\{ar^2\left(ar^2+3\right) + 1\right\}. \tag{38}$$

Since the coupling constant α and the background cloud density Θ are always in product form, the background density can be tuned either by α or by Θ. Now, the rest of the physical parameters can be derived from the above three thermodynamic quantities. The pressure anisotropy can be determined as $\Delta = p_t - p_r$. The variation of density, pressures, and

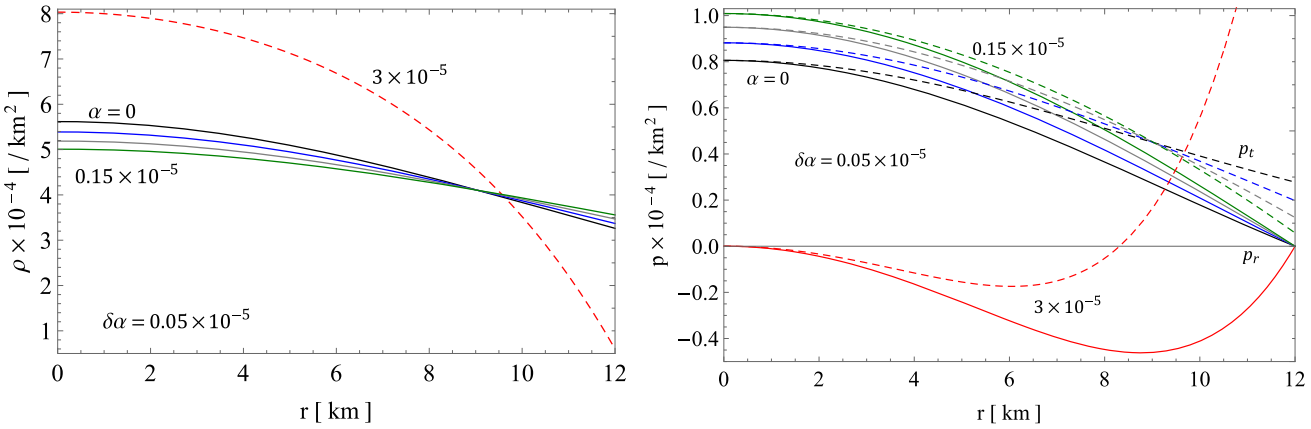

Fig. 1 Density and pressure for different α with $M = 2M_{\odot}$, $R = 12$ km and $\Theta = 50$

pressure anisotropy with respect to the radial coordinate is shown in Figs. 1 and 2 (left). From Fig. 1 (left), one can see that the central density decreases as α increases from 0 to 0.15×10^{-5}; however, it increases when $\alpha = 3\times10^{-5}$. This is because, from Eq. (36), we can see that the density in the interior decreases as $-e^{-cr^2}/r^2$, which dominates over the term $+\alpha\,\Theta$ when α is very small in the range $[0, , 0.15 \times 10^{-5}]$. However, when the α parameter shifts to a larger value of 3×10^{-5}, the second term adds a significant central density, thus leading to a higher central density.

The causality condition can be investigated via the speed of sound in the radial and transverse components, given by

$$v_r^2 = \frac{dp_r}{d\rho} \quad \text{and} \quad v_t^2 = \frac{dp_t}{d\rho}. \tag{39}$$

In Fig. 2 (right), one can see that the causality condition holds for $\alpha < 3 \times 10^{-5}$. For $\alpha = 3 \times 10^{-5}$, the values of v_s^2 are less than 0 for radii above 6 km, signifying that the speed of sound is unphysical (or imaginary). The reason behind the imaginary value of the sound speed is related to the collapsing state, which will be discussed in the coming section.

4 Boundary conditions

The interior metric (10) inside the compact star should be joined continuously with the exterior metric. Due to the background uniform density cloud, the exterior spacetime must differ from the Schwarzschild vacuum. For a uniform density background dust, the field equation (24) takes the form

$$\mathrm{e}^{-\lambda}\left(\frac{\lambda'}{r} - \frac{1}{r^2}\right) + \frac{1}{r^2} = 8\pi\alpha\,\Theta \quad \forall\ r > R, \tag{40}$$

whose solution is found to be

$$e^{-\lambda} = 1 - \frac{c_1}{r} - \frac{8\pi}{3}\alpha\,\Theta\,r^2, \tag{41}$$

where $c_1 = 2M$; however, due to the extremely thin cloud density, one can always assume the Schwarzschild vacuum, i.e.

$$ds^2 = \left[1 - \frac{2m}{r}\right]dt^2 - \frac{dr^2}{1-2m/r} - r^2\left(d\theta^2 + \sin^2\theta\,d\phi^2\right), \tag{42}$$

with the radial coordinate r being greater than $2m$. At the surface ($r = R$), we get [44]

$$1 - \frac{2M}{R} = e^{\nu_s} = e^{-\lambda_s}. \tag{43}$$

Further, the extrinsic curvature $K_{\mu\nu} = \nabla_\mu \hat{r}_\nu$ (where $\hat{r}_\mu$ is the unit radial vector normal to any surface of radius r) is also required to be continuous at the interface ($r = R$) or equivalently [45],

$$[G_{\mu\nu}\hat{r}^\nu]_s = \lim_{r\to R^+}(G_{\mu\nu}\,\hat{r}^\nu) - \lim_{r\to R^-}(G_{\mu\nu}\,\hat{r}^\nu) = 0. \tag{44}$$

By using the field equations and Eq. (44), we obtain

$$\left[8\pi\ T_{\mu\nu}\,\hat{r}^\nu\right]_s = 0, \tag{45}$$

which implies

$$\left[8\pi\left(\tilde{p}_r - \alpha\ \Theta_r^r\right)\right]_s = 0,$$

$$\text{Or}\ \ \tilde{p}_r(R) - \alpha\ \Theta_r^r(r \to R^-) = 0. \tag{46}$$

By considering the boundary conditions (43) and (46), we find

$$c = -\frac{1}{R^2}\ln\left(1 - \frac{2M}{R} + \frac{8\pi}{3}\alpha\,\Theta R^2\right), \tag{47}$$

$$a = \frac{3 - e^{cR^2}\left(8\pi\alpha\,\Theta R^2 + 3\right)}{2R^2\left(8\pi\alpha\,\Theta R^2\,e^{cR^2} - 3\right)}, \tag{48}$$

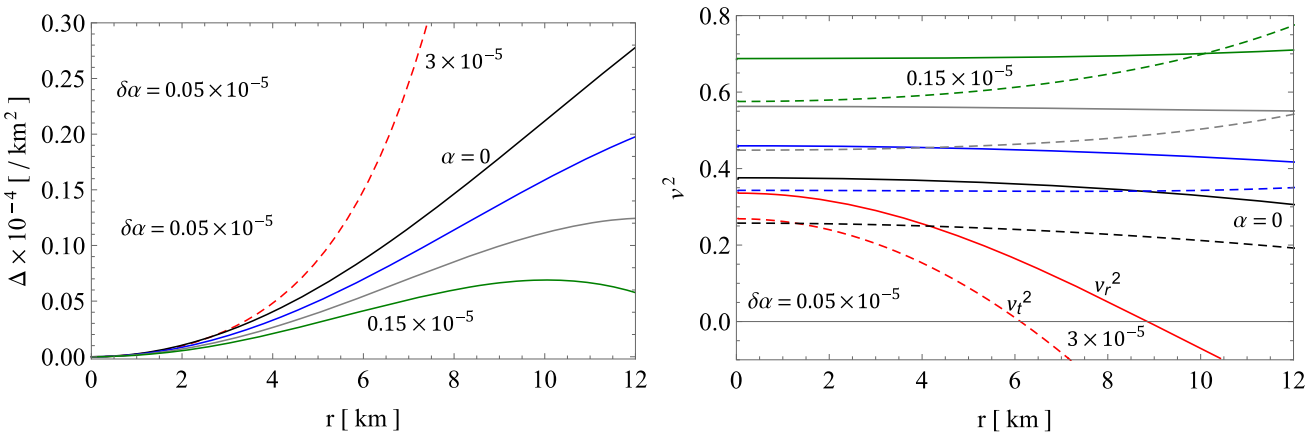

Fig. 2 Anisotropy and square of sound speed for different α with $M = 2M_{\odot}$, $R = 12$ km and $\Theta = 50$

$$b = \ln\left(1 - \frac{2M}{R}\right) - aR^2. \tag{49}$$

Here, M, R and Θ will be chosen manually, with α serving as a tuning parameter.

5 Hydrostatic equilibrium, radial perturbations, the adiabatic index, and stability

5.1 Hydrostatic equilibrium

To achieve equilibrium in the stellar fluid system, the forces acting on the system must counterbalance each other in the modified TOV equation, i.e.,

$$-\frac{d\tilde{p}_r}{dr} - \frac{\nu'}{2}(\tilde{\rho} + \tilde{p}_r) + \frac{2(\tilde{p}_t - \tilde{p}_r)}{r} - \alpha\left[\frac{\nu'}{2}(\Theta_t^t - \Theta_r^r) - \frac{d\Theta_r^r}{dr} + \frac{2}{r}(\Theta_\varphi^\varphi - \Theta_r^r)\right] = 0. \tag{50}$$

Counterbalancing these forces can be observed in Fig. 3 where the effective gravitational force $F_g = -\frac{\nu'}{2}(\tilde{\rho} + \tilde{p}_r) - \frac{\nu'}{2}\alpha(\Theta_t^t - \Theta_r^r)$ counterbalances the combined forces of anisotropy, $F_a = \frac{2(\tilde{p}_t - \tilde{p}_r)}{r} - \alpha\frac{2}{r}(\Theta_\varphi^\varphi - \Theta_r^r)$ and hydrostatic pressure, $F_h = -\frac{d\tilde{p}_r}{dr} + \alpha\frac{d\Theta_r^r}{dr}$. Thus, the system is in hydrostatic equilibrium.

5.2 Radial perturbations, adiabatic index, and stability

A compact stellar system embedded in a background filled with matter or clouds can significantly affect its stability. The background cloud, coupled to the geometry of spacetime, can be adjusted using the MGD parameter α. A slight radial perturbation may be triggered when a low-density background cloud accretes onto the compact star.

As the compact star is embedded in a background filled with a uniform density cloud, it is not difficult to imagine

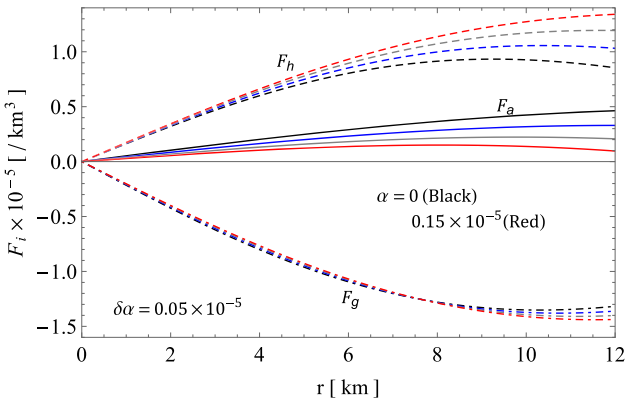

Fig. 3 Forces in TOV for different α with $M = 2M_{\odot}$, $R = 12$ km and $\Theta = 50$

that some mass may be falling onto the compact star, inducing a small density perturbation. Assuming this perturbation occurs only along the radial direction, then according to Harrison et al. [46] and Zel'dovich-Novikov [47], the mass of the compact star must be an increasing function of the central density (i.e., $dM/d\rho_0 > 0$) in a non-collapsing state (i.e., stable). The mass as a function of the central density ρ_0 is given by

$$M(\rho_0) = \frac{R}{2}\left(1 - e^{-8\pi R^2(\rho_0 - \alpha\Theta)/3} + \frac{8\pi}{3}\alpha\Theta R^2\right). \tag{51}$$

Here, R is the surface radius. The variation of mass with central density is shown in Fig. 4 (left), which is an increasing function of ρ_0, indicating stability under radial density fluctuations. It can also be observed that as the background cloud adds more mass (i.e., more α), the configuration gains additional mass. This signifies that the system can support more mass for the same ρ_0 as α increases. In other words, adding more mass from the cloud helps the system achieve a more stable configuration. However, to gain a deeper understanding, one must also consider the corresponding adiabatic

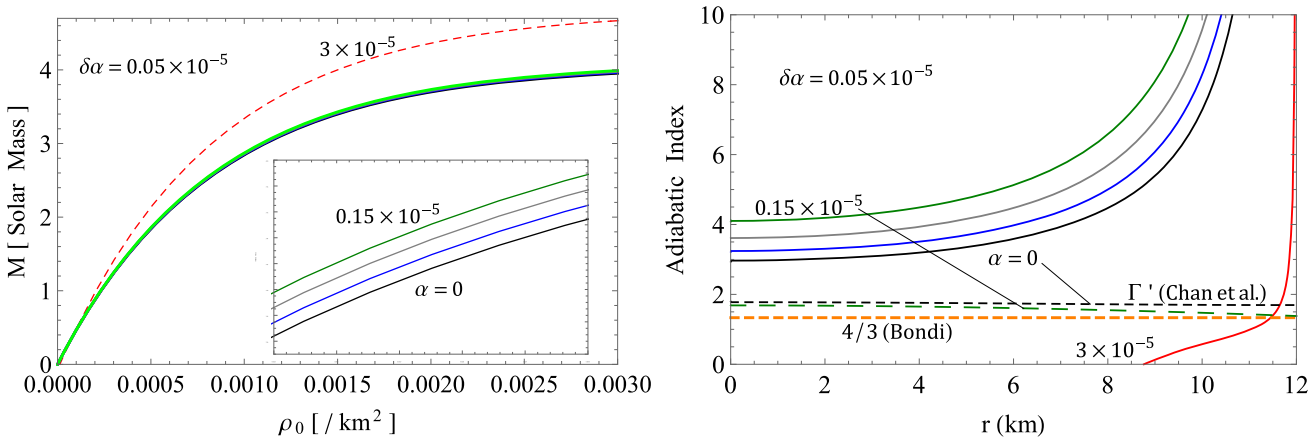

Fig. 4 Mass vs central density and adiabatic index for different α with $M = 2M_\odot$, $R = 12$ km and $\Theta = 50$

index defined by

$$\Gamma = \frac{\rho + p_r}{p_r}\frac{dp_r}{d\rho}. \tag{52}$$

The variation of Γ is shown in Fig. 4 (right), and it is clear that it is greater than $\frac{4}{3}$ for $\alpha = 0$ to 0.15×10^{-5} and less than $\Gamma_B = \frac{4}{3}$ for $\alpha = 3\times10^{-5}$. According to Bondi's condition [48], this system will collapse if $\Gamma < \frac{4}{3}$. The extension of this similar condition was proposed by Chan et al. [49] for anisotropic fluid as

$$\Gamma_B < \Gamma' = \frac{4}{3}\left(1 + \frac{\{4\Delta + \rho r^2 p_r\}}{4r\,|(p_r)|'}\right)_{max}, \tag{53}$$

where Γ' is the new adiabatic index limit that redefines Bondi's limit, and Γ'_{max} is the maximum value below which the system will collapse. The variations of Γ' are also shown in Fig. 4 (right), which are above the Γ_B line. Here, for $\alpha = 0$, the maximum is $\Gamma'_{max} = 1.773$, which is above Bondi's limit $\Gamma_B = \frac{4}{3}$. All the adiabatic indices Γ for $\alpha = 0 - 0.15\times10^{-5}$ are above Γ'_{max} and hence stable under radial perturbations, while for $\alpha \geq 3\times10^{-5}$, $\Gamma < \Gamma'_{max}$ and hence unstable. This means that if the mass falling from the surrounding uniform density cloud exceeds a maximum limit, the system will trigger gravitational collapse. Increasing in-falling mass implies an increase in the background density $\rho_\Theta = \alpha\,\Theta$. Hence, the perturbation induced by the background cloud increases with the increase in the background density, which easily alters the stability of the compact star.

6 Fitting of a few observed masses on $M - R$ curve

To check whether the solution is adapted to the observed astrophysical scenario, one must accommodate the observed masses and predict the radius, which must be within the observed range. The $M - R$ curve from this solution is shown in Fig. 5. Here, one can see that the mass and the corresponding radius increase with the increase in coupling strength α (or increase in effective cloud density). Further, for a few massive compact stars, we have fitted the observed mass and used their uncertainties to predict the range of radii for different values of α in Table 1 by using the $M - R$ curve. The overall predicted range is $R_{pred} \in [10, 12.05]$ km. One can also clearly see from the $M - R$ curve that the compact object in GW200210 lies above and below the Buchdahl limit when the uncertainty range $2.83^{+0.47}_{-0.42}M_\odot$ is used. This means that the object (as of now unknown) lies within the NS-black hole interface known as the "mass gap." If the compact object in GW200210 has the upper limit mass, i.e., $2.83 + 0.47 = 3.3M_\odot$ at a radius below 10.96 km (Buchdahl radius), then the object will collapse and form a black hole at a Schwarzschild radius $R_{BH} = 9.746$ km. However, if the lower mass, i.e., $2.83 - 0.42 = 2.41M_\odot$, is taken, then the compact object in GW200210 is more likely a massive NS

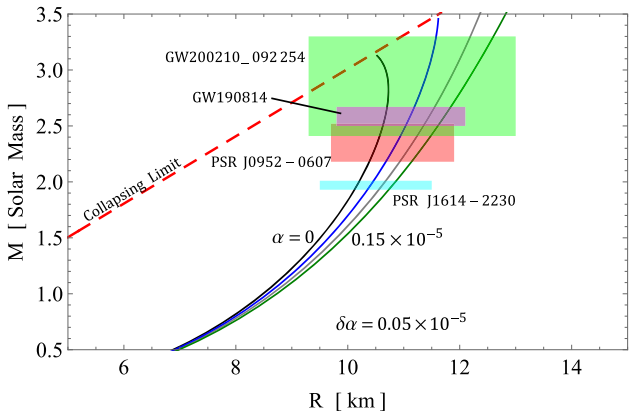

Fig. 5 $M - R$ curve for different α with $M = 2M_\odot$, $R = 12$ km and $\Theta = 50$

Table 1 Estimated radii of a few high-mass compact objects as shown in Fig. 5

Objects	$\frac{M}{M_\odot}$	Predicted R (km)			
		$\alpha \times 10^{-5}$			
		0	0.05	0.10	0.15
PSR J1614-2230 [50]	1.97 ± 0.04	$10.15^{+0.05}_{-0.03}$	$10.39^{+0.07}_{-0.03}$	$10.61^{+0.06}_{-0.04}$	$10.81^{+0.05}_{-0.07}$
PSR J0952-0607 [51]	2.35 ± 0.17	$10.52^{+0.11}_{-0.14}$	$10.87^{+0.18}_{-0.19}$	$11.17^{+0.46}_{-0.25}$	$11.39^{+0.24}_{-0.14}$
GW190814 [52]	$2.5 - 2.67$	$10.66^{+0.03}_{-0.04}$	$11.10^{+0.09}_{-0.07}$	$11.44^{+0.12}_{-0.09}$	$11.70^{+0.14}_{-0.08}$
GW200210 [53]	$2.83^{+0.47}_{-0.42}$	$10.74^{-}_{-0.17}$	$11.31^{+0.29}_{-0.35}$	$11.72^{+0.46}_{-0.45}$	$12.05^{+0.55}_{-0.55}$

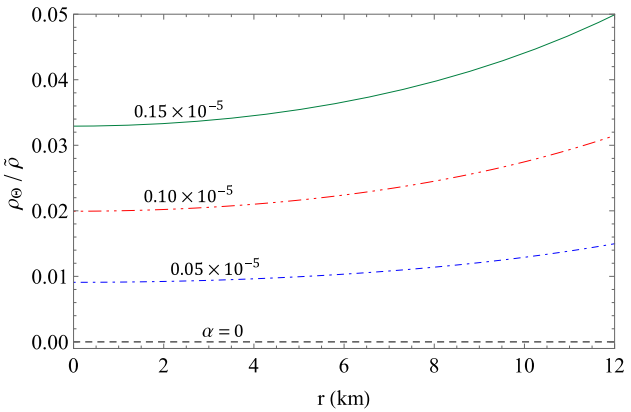

Fig. 6 Variation of the dark matter density to the normal matter density ratio with respect to r

since $R_{BH} = 7.12$ km is far below the range of NS radius. For the rest of the objects, we have predicted the radii.

7 Final remarks

In this work, we have imagined a scenario where compact objects, mostly NSs, are surrounded by a thin uniform cloud similar to planetary nebulae-type environments, and how the stability of NSs can be altered due to the addition of a small mass from the thin cloud. One interesting observation is that if the surrounding cloud density is at least 5% of the NS surface density, i.e., $\frac{\rho_\Theta(R)}{\tilde{\rho}(R)} = 0.05$ (for $\alpha = 0.15 \times 10^{-5}$; see Fig. 6), then the additional mass from the cloud becomes significant in altering the stability of the NS. When α approaches 3×10^{-5}, the density ratio will be above 5%, triggering instability. This instability may lead to a density perturbation sufficient enough to initiate a gravitational collapse. Also, as α approaches 3×10^{-5}, the adiabatic index crosses $\Gamma'_{\rm max}$ leading to gravitational collapse. Due to the increase in pressure while increasing α, more exotic processes can be initiated, generating more anisotropy in pressure. In the range $0 \leq \alpha < 3 \times 10^{-5}$, the compact system is still in equilibrium, follows causality, is stable under small pressure and density fluctuations, and is also supported by a sufficiently stiff fluid with $\Gamma > \Gamma'_{\rm max} = 1.773$.

The $M - R$ curve and Table 1 determine the radii of some massive NSs for different values of background cloud density. From here, it can also be concluded that the compact object in GW200210 is clearly within the NS-BH mass gap. This object can be a stellar BH if the upper limit mass $3.3 M_\odot$ is taken. Its Buchdahl radius of 9.746 km is within the NS range and hence can be confused with a massive NS. Although, if the lower mass $2.41 M_\odot$ is taken, then the compact object in GW200210 is more likely a massive NS, as $R_{\rm BH} = 7.12$ km is far below the range of NSs. For the rest of the NSs, we have predicted the radii for different surrounding cloud densities.

Acknowledgements AE thanks the National Research Foundation of South Africa for the award of a postdoctoral fellowship. The authors S. K. Maurya and Smitha TT thank the administration of the University of Nizwa in the Sultanate of Oman for their constant support and encouragement in conducting this work.

Funding This research was funded by the Science Committee of the Ministry of Science and Higher Education of the Republic of Kazakhstan (Grant No. AP23487178).

Data Availability Statement My manuscript has no associated data. (There is no observational data related to this article. The necessary calculations and graphic discussion can be made available on request.)

Code Availability Statement My manuscript has no associated code/software. [Authors' comment: Code/Software sharing not applicable to this article as no code/software was generated or analysed during the current study.]

Declarations

Conflict of interest The authors declare that they have no known competing financial interests or personal relationships that could have appeared to influence the work reported in this paper.

Funded by SCOAP[3].

References

1. J.M. Lattimer, M. Prakash, Science **304**, 536–542 (2004)
2. J.M. Lattimer, Ann. Rev. Nucl. Part. Sci. **62**, 485–515 (2012)
3. F. Ozel, D. Psaltis, T. Guver, G. Baym, C. Heinke, S. Guillot, Astrophys. J. **820**(1), 28 (2016)
4. S. Ray, S. Bhadra, Phys. Lett. A **322**, 150–155 (2004)
5. F. Rahaman, P.K.F. Kuhfittig, R. Amin, G. Mandal, S. Ray, N. Islam, Phys. Lett. B **714**, 131–135 (2012)
6. S. Saklany, N. Pant, B. Pandey, Phys. Lett. B **845**, 138176 (2023)
7. J.S. Read, B.D. Lackey, B.J. Owen, J.L. Friedman, Phys. Rev. D **79**, 124032 (2009)
8. A. Kurkela, E.S. Fraga, J. Schaffner-Bielich, A. Vuorinen, Astrophys. J. **789**, 127 (2014)
9. E. Annala, T. Gorda, A. Kurkela, A. Vuorinen, Phys. Rev. Lett. **120**(17), 172703 (2018)
10. E.R. Most, L.R. Weih, L. Rezzolla, J. Schaffner-Bielich, Phys. Rev. Lett. **120**(26), 261103 (2018)
11. M.G. Alford, S. Han, M. Prakash, Phys. Rev. D **88**(8), 083013 (2013)
12. P. Bedaque, A.W. Steiner, Phys. Rev. Lett. **114**(3), 031103 (2015)
13. S.K. Greif, G. Raaijmakers, K. Hebeler, A. Schwenk, A.L. Watts, Mon. Not. R. Astron. Soc. **485**(4), 5363–5376 (2019)
14. I. Tews, J. Carlson, S. Gandolfi, S. Reddy, Astrophys. J. **860**(2), 149 (2018)
15. E. Annala, T. Gorda, A. Kurkela, J. Nättilä, A. Vuorinen, Nat. Phys. **16**(9), 907–910 (2020)
16. L. Lindblom, Phys. Rev. D **82**, 103011 (2010). https://doi.org/10.1103/PhysRevD.82.103011. arXiv:1009.0738 [astro-ph.HE]
17. B.P. Abbott et al. [LIGO Scientific and Virgo], Phys. Rev. Lett. **121**(16), 161101 (2018)
18. L. Lindblom, Phys. Rev. D **105**(6), 063031 (2022)
19. P. Landry, R. Essick, K. Chatziioannou, Phys. Rev. D **101**(12), 123007 (2020)
20. I. Legred, K. Chatziioannou, R. Essick, S. Han, P. Landry, Phys. Rev. D **104**(6), 063003 (2021)
21. J. Ovalle, Phys. Rev. D **95**, 104019 (2017)
22. J. Ovalle, A. Sotomayor, Eur. Phys. J. Plus **133**, 428 (2018)
23. C. Las Heras, P. León, Eur. Phys. J. C **79**, 990 (2019)
24. S.K. Maurya, K.N. Singh, M. Govender, S. Hansraj, Astrophys. J. **925**(2), 208 (2022)
25. M. Sharif, S. Iltaf, Chin. J. Phys. **79**, 173–191 (2022)
26. S.K. Maurya, K.N. Singh, M. Govender, G. Mustafa, S. Ray, Astrophys. J. Suppl. **269**(2), 35 (2023)
27. S.K. Maurya, A. Errehymy, M. Govender, G. Mustafa, N. Al-Harbi, A.H. Abdel-Aty, Eur. Phys. J. C **83**(4), 348 (2023)
28. S.K. Maurya, F. Tello-Ortiz, M. Govender, Fortsch. Phys. **69**(10), 2100099 (2021)
29. H. Azmat, M. Zubair, Eur. Phys. J. Plus **136**(1), 112 (2021)
30. H. Azmat, M. Zubair, Z. Ahmad, Ann. Phys. **439**, 168769 (2022)
31. D. Santana, E. Fuenmayor, E. Contreras, Eur. Phys. J. C **82**(8), 703 (2022)
32. R. Casadio, E. Contreras, J. Ovalle, A. Sotomayor, Z. Stuchlick, Eur. Phys. J. C **79**(10), 826 (2019)
33. J. Ovalle, R. Casadio, R. da Rocha, A. Sotomayor, Eur. Phys. J. C **78**(2), 122 (2018)
34. J. Ovalle, R. Casadio, R. da Rocha, A. Sotomayor, Z. Stuchlik, EPL **124**(2), 20004 (2018)
35. L. Gabbanelli, J. Ovalle, A. Sotomayor, Z. Stuchlik, R. Casadio, Eur. Phys. J. C **79**(6), 486 (2019)
36. J. Ovalle, C. Posada, Z. Stuchlík, Class. Quantum Gravity **36**(20), 205010 (2019)
37. S.K. Maurya, A. Banerjee, A. Pradhan, D. Yadav, Eur. Phys. J. C **82**(6), 552 (2022)
38. J. Ovalle, Phys. Lett. B **788**, 213 (2019)
39. K.D. Krori, J. Barua, J. Phys. A Math. Gen. **8**, 508 (1975)
40. M. Zubair, G. Abbas, I. Noureen, Astrophys. Space Sci. **361**, 8 (2016)
41. G. Abbas, S. Qaisar, A. Jawad, S. Qaisar, A. Jawad, Astrophys. Space Sci. **359**, 57 (2015)
42. M.F. Shamir, S. Zia, Eur. Phys. J. C **77**, 448 (2017)
43. Z. Yousaf, M.Z.u.H. Bhatti, M. Ilyas, Eur. Phys. J. C **78**, 307 (2018)
44. W. Israel, Nuovo Cim. B **44**, 1 (1966)
45. N.O. Santos, Mon. Not. R. Astron. Soc. **216**, 403 (1985)
46. B.K. Harrison, K.S. Thorne, M. Wakano, J.A. Wheeler, *Gravitational Theory and Gravitational Collapse* (University of Chicago Press, Chicago, 1965), p.119
47. Y.B. Zeldovich, I.D. Novikov, *Relativistic Astrophysics Stars and Relativity*, vol. 1 (University of Chicago Press, Chicago, 1971)
48. H. Bondi, Proc. R. Soc. Lond. Ser. A Math. Phys. Eng. Sci. **281**, 39 (1964)
49. R. Chan, L. Herrera, N.O. Santos, Mon. Not. R. Astron. Soc. **265**, 533 (1993)
50. P.B. Demorest, T. Pennucci, S. Ransom, M. Roberts, J. Hessels, Nature **467**, 1081 (2010)
51. R.W. Romani, D. Kandel, A.V. Filippenko, T.G. Brink, W. Zheng, Astrophys. J. Lett. **934**, L18 (2022)
52. R. Abbott et al., Astrophys. J. Lett. **896**, L44 (2020)
53. R. Abbott et al., Phys. Rev. X **13**, 041039 (2023)